Comparing Conventional and Buffered Failure Probability from the Perspective of Risk-based Decision-Making

Uichan Seok
Graduate Student, Dept. of Civil & Environmental Engineering, Seoul National University, Seoul, South Korea

Ji-Eun Byun
Lecturer, James Watt School of Engineering, University of Glasgow, Glasgow, United Kingdom

Junho Song
Professor, Dept. of Civil & Environmental Engineering, Seoul National University, Seoul, South Korea

ABSTRACT: Failure probability has been widely used as a reliability metric to provide a building block of reliability-based decision-making. Such use of failure probability has implications for both risk management and computation. In this study, we revisit the familiar concept of a reliability metric by comparing *the conventional failure probability* with a recently proposed alternative metric, *the buffered failure probability*. Comparisons are made from the perspectives of risk management, failure probability evaluation, and reliability-based optimization. In addition to analytical examinations, we present numerical investigations revealing several intriguing distinctions between the failure probabilities. We also contemplate the prospects of using the two metrics in parallel.

1. INTRODUCTION

In order to secure the reliability of an engineering system against hazardous events, one needs to make risk-informed decisions by taking into account uncertainties. In order to perform such a task, one first needs to define a reliability metric. One of the most common metrics in reliability engineering is *failure probability.* When using a failure probability, the design objective is effectively controlling undesirable events, i.e., *failure events.* Numerous system reliability analysis methods have been developed to enable efficient evaluation of failure probability by exploiting the definition of the conventional failure probability.

While the conventional definition of failure probability has been widely used, an alternative reliability metric, buffered failure probability, has recently been proposed (Rockafellar and Royset, 2010). Stemming from the *conditional value-at-risk* (CVaR) (Rockafellar and Uryasev, 2000; Rockafellar and Uryasev, 2002), widely used in finance, economics, and operations research, the buffered failure probability has a fundamentally equivalent perspective of risk management to the conventional definition in that it focuses on the worst-case events (i.e., failure events). On the other hand, evaluating this alternative metric requires a distinctive formula, resulting in different computational characteristics.

In this study, we compare the conventional and buffered failure probabilities. We intend to revisit and contemplate the familiar concept of failure probability from both decision-making and computational efficiency perspectives. The paper is organized as follows. First, Section 2 presents illustrative definitions of the two failure probabilities and compares them from the perspective of risk management. Then, Section 3 presents their mathematical definitions and compares them in terms of computational efficiency. The section also compares the performance of the Monte Carlo Simulation in computing the failure probabilities. Section 4 presents a comparison from the reliability-based optimization perspective. We analyze the

computational advantages of the optimization formulas and present a numerical example to compare optimization solutions obtained with the two metrics. Finally, Section 5 presents concluding remarks and future research topics.

2. CONVENTIONAL AND BUFFERED FAILURE PROBABILITY AS RELIABILITY METRICS

Failure events refer to undesirable events, often defined in terms of a reference value on the system state. Then, failure probability is defined as the probability of failure events. In this paper, without loss of generality, we assume that a higher system state indicates a worse scenario, and a reference value is set to 0. Conventionally, such a reference value is considered a fixed threshold, whereby an event is considered a failure when the corresponding system state is greater than the value. On the other hand, an alternative definition of failure probability has been recently proposed (Rockafellar and Royset, 2010), namely *buffered failure probability*. The buffered failure probability considers a provided reference value as the expectation of the worst (i.e., highest) system states, which become failure events. In other words, the failure events are the events that contribute to the expectation and can have a system state lower than a given reference value.

From the decision theory perspective, treating the reference value determines decision objectives (Rockafellar and Royset, 2015). The conventional failure probability considers that all events with the system state beyond 0 are equally "negative." This is equivalent to defining a loss function as constant for all system states beyond 0. Then, the decision objective is to control the occurrence of any of those events. On the other hand, as the buffered failure probability considers the expectation of a system event's right tail, the loss function increases linearly over failure events. From the decision-making perspective, a given reference value is considered a budget set aside to cope with the worst scenarios. The decision objective is to control the occurrence of losses beyond the budget.

Such different views on failure events enable choosing the failure probability concept more suitable for a given problem. The conventional definition is more suitable for problems where the magnitude of the system state under failure does not play a significant role. For example, a structural system is considered failing if a load exceeds a capacity, regardless of the difference. On the other hand, the buffered failure probability is more suitable for problems for which such magnitude matters. Examples include financial losses or casualties.

As the buffered failure probability considers a system state's magnitude, it is not invariant to the formula of a limit-state function, in contrast to the conventional failure probability. For example, for two limit-state functions $g_1(\boldsymbol{V}) = V_1 - V_2$ and $g_1(\boldsymbol{V}) = V_1/V_2 - 1$, the conventional failure probability returns the same value, while it is not the case for the buffered failure probability. One may choose between the two metrics depending on a given problem.

These two similar but different reliability metrics show strong positive correlations (Byun and Royset, 2022). The buffered failure probability is always greater than or equal to the conventional failure probability. The lighter the thickness of the right tail, the smaller the difference is. If the system state follows the standard normal distribution, the ratio of the two metrics is around 2.7.

3. CALCULATION OF FAILURE PROBABILITY

3.1. Formulas

Consider a limit-state function $g(\boldsymbol{x}, \boldsymbol{V})$ with design variables $\boldsymbol{x} = (x_1, x_2, \cdots, x_n)$ and random variables $\boldsymbol{V} = (V_1, V_2, \cdots, V_m)$. The random variable V_g represents the value of $g(\boldsymbol{x}, \boldsymbol{V})$. In the following, the formulas of the two failure probabilities are explained and compared using quantile and superquantile.

The conventional failure probability, denoted as p_f, is computed as

$$\begin{aligned} p_f &= P[V_g > 0] \\ &= 1 - F_{V_g}(q_{\alpha_0}) \\ &= 1 - \alpha_0, \end{aligned} \tag{1}$$

where $F_{V_g}(\cdot)$ is the cumulative distribution function (CDF), and

$$q_{\alpha_0} = 0. \tag{2}$$

On the other hand, the buffered failure probability, denoted as $\bar{p}_f$, is calculated as

$$\begin{aligned} \bar{p}_f &= P[V_g > q_{\bar{\alpha}_0}] \\ &= 1 - F_{V_g}(q_{\bar{\alpha}_0}) \\ &= 1 - \bar{\alpha}_0, \end{aligned} \tag{3}$$

where the quantile value $q_{\bar{\alpha}_0}$ has a superquatile value $\bar{q}_{\bar{\alpha}_0} = 0$, i.e.,

$$\bar{q}_{\bar{\alpha}_0} = \mathbb{E}[V_g | V_g \geq q_{\bar{\alpha}_0}] = 0. \tag{4}$$

Comparison of Eqs. (2) and (4) shows how the reference value 0 is treated differently by the conventional and buffered failure probability.

Figure 1 compares the terms in Eqs. (1)-(4) by assuming that V_g follows the normal distribution with a mean of -1 and a standard deviation of 1. In the figure, the conventional failure probability p_f is calculated as 0.16 with a threshold $q_{\alpha_0} = 0$. On the other hand, the buffered failure probability $\bar{p}_f$ is computed as 0.38, where the threshold $q_{\bar{\alpha}_0} = -0.70$ is obtained from $\mathbb{E}[V_g | V_g \geq -0.70] = 0$. The figure shows how the buffered failure probability places a buffered zone below 0.

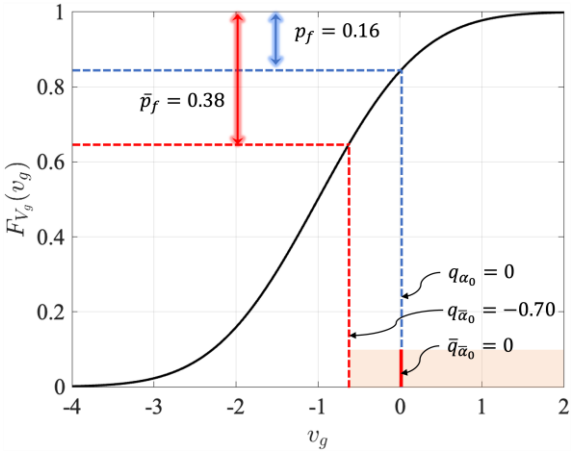

Figure 1: The conventional and buffered failure probability in the illustrative example.

In an *n*-dimensional problem, the failure probability is evaluated as

$$\begin{aligned} p_f = \int \cdots \int \mathbb{I}[g(\boldsymbol{x}, \boldsymbol{v}) > q_{\alpha_0}] \\ \times f_{\boldsymbol{V}}(\boldsymbol{v}) dv_1 \cdots dv_m, \end{aligned} \tag{5}$$

$$\begin{aligned} \bar{p}_f = \int \cdots \int \mathbb{I}[g(\boldsymbol{x}, \boldsymbol{v}) > q_{\bar{\alpha}_0}] \\ \times f_{\boldsymbol{V}}(\boldsymbol{v}) dv_1 \cdots dv_m, \end{aligned} \tag{6}$$

where $\mathbb{I}[\cdot]$ is the indicator function, and $f_{\boldsymbol{V}}(\boldsymbol{v})$ denotes the joint probability density function (PDF) of $\boldsymbol{V}$.

3.2. Monte Carlo Simulation

3.2.1. Formulas

When the joint PDF of random variables is complex and high-dimensional, the calculation of a failure probability can become intractable. This issue can be resolved by employing sampling techniques, for which the most basic technique is Monte Carlo Simulation (MCS). Specifically, by generating N Monte Carlo (MC) samples, $v_g^1, \ldots, v_g^N$, the conventional and buffered failure probabilities are respectively estimated as

$$p_f = \frac{1}{N} \sum_{i=1}^{N} \mathbb{I}[v_g^i \geq 0], \text{and} \tag{7}$$

$$\bar{p}_f = \frac{1}{N} \sum_{i=1}^{N} \mathbb{I}[v_g^i > q_{\bar{\alpha}_0}]. \tag{8}$$

It is noted that, in contrast to the conventional failure probability, the buffered failure probability requires computing $q_{\bar{\alpha}_0}$ beforehand. This can be done by sorting $v_g^1, \dots, v_g^N$ in the descending order, and compute (Mafusalov and Uryasev, 2018)

$$\bar{p}_f \cong \frac{1}{N}\sum_{i=n^*+1}^{N}\left(\frac{v_g^i - v_g^{n^*}}{-v_g^{n^*}}\right), \tag{9}$$

where $v_g^i \geq v_g^j$ for all $i > j$, and n^* is an index that satisfies

$$\sum_{i=n^*}^{N} v_g^i < 0 < \sum_{i=n^*+1}^{N} v_g^i. \tag{10}$$

In other words, $v_g^{n^*}$ is a numerical estimation of $q_{\bar{\alpha}_0}$ in Eq. (6).

3.2.2. Numerical investigation of convergence

To demonstrate the implementation of MCS for the two failure probabilities, we investigate four problems with limit-state functions

$$g_1(\alpha_1, \boldsymbol{V}) = -\alpha_1 + \frac{1}{\sqrt{M}}\sum_{i=1}^{M} V_i, \tag{11}$$

$$g_2(\alpha_2, \kappa, \boldsymbol{V}) = -\alpha_2 + \frac{1}{\sqrt{M}}\sum_{i=1}^{M} V_i - \frac{\kappa}{4}(V_1 - V_2)^2, \tag{12}$$

$$g_3(\alpha_3, \boldsymbol{V}) = -\frac{\alpha_3}{|V_2|} + V_1, \text{and} \tag{13}$$

$$g_4(r, m, \boldsymbol{V}) = -1 + \frac{\|\boldsymbol{V}\|^2}{r^2} + \frac{V_1}{r}\frac{1 - (\|\boldsymbol{V}\|/r)^m}{1 + (\|\boldsymbol{V}\|/r)^m}, \tag{14}$$

where $\alpha_1 = \alpha_2 = \alpha_3 = \Phi^{-1}(0.99)$, $M = 2$, $\kappa = 1$, $r = 3$, and $m = 4$ (Betz, 2017). We perform MCS for each limit-state function by varying the sample size from 10^2 to 10^4. The mean and ± 1 standard deviation range of each metric are calculated.

The results are summarized in Figures 2 and 3. Figure 2 shows the 10^4 MC samples and the failure domains estimated for the four limit-state functions. Specifically, the blue line that represents the conventional failure probability denotes the line of $V_g = 0$, while the red line that stands for the buffered failure probability represents the estimated line of $V_g = q_{\bar{\alpha}_0}$. Meanwhile, Figure 3 shows the convergence of the two failure probabilities as the sample size increases. Both figures show that the buffered failure probability leads to a larger failure domain and a greater failure probability.

A noteworthy observation in Figure 3 is that the buffered failure probability is consistently underestimated with a small sample size. All red lines in the figure are below the exact values before the sample size reaches 10^3. By contrast, MCS produces unbiased estimates of the conventional failure probability.

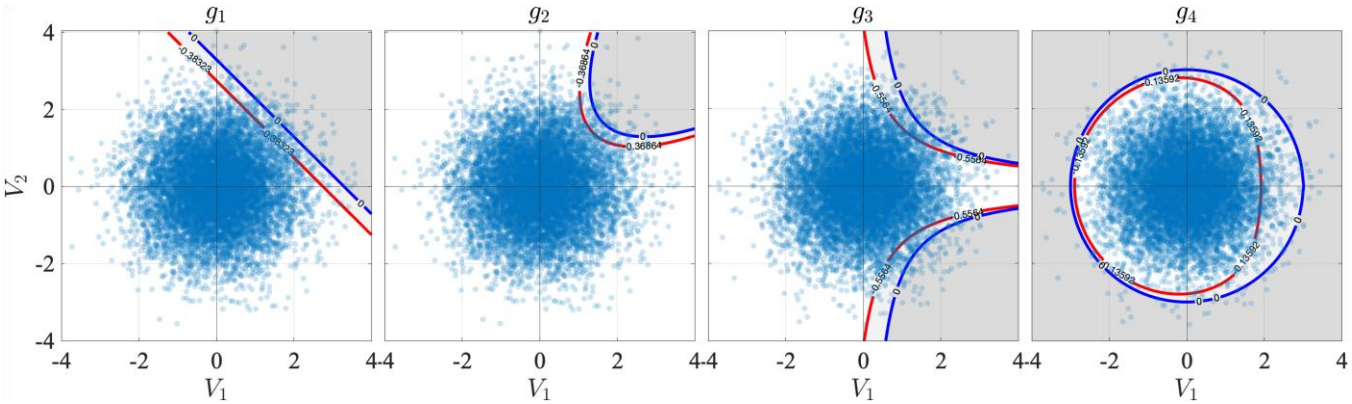

Figure 2: Threshold values of the failure domains estimated with 10^4 samples, respectively, for g_1, g_2, g_3, and g_4 from left to right. The red and blue lines represent the values for $\bar{p}_f$ and p_f, respectively.

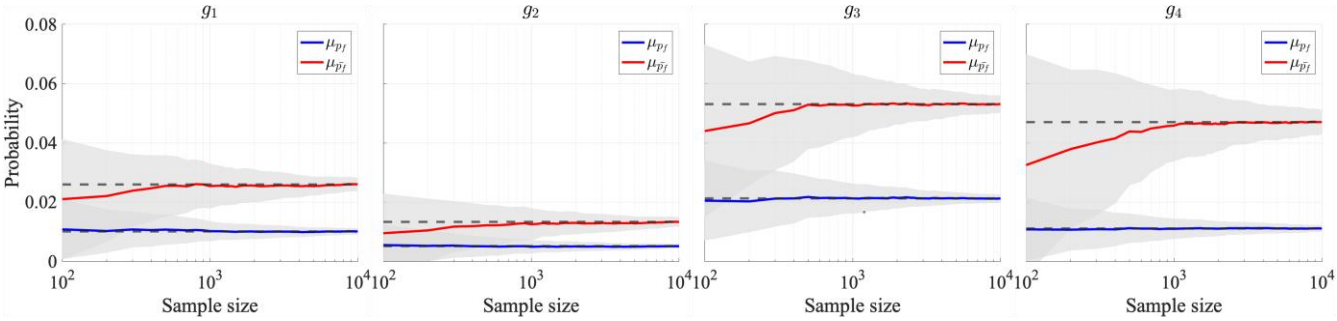

Figure 3: Convergence of estimations for p_f and $\bar{p}_f$ for g_1, g_2, g_3, and g_4 from left to right. The red and blue lines represent the mean estimations of $\bar{p}_f$ and p_f, respectively, the gray shades indicate a $\pm\sigma$ range of each estimation, and the dotted lines show the exact values.

4. RELIABILITY-BASED OPTIMIZATION

4.1. Formulas

Conventionally, reliability-based optimization (RBO) aims to minimize a cost function while satisfying reliability constraints, which can be formulated as

$$\begin{aligned} &\min_{\boldsymbol{x}} c(\boldsymbol{x}) \\ &\text{s.t. } p_f(\boldsymbol{x}) \le p_f^t \\ &\quad \boldsymbol{x} \in \boldsymbol{X}, \end{aligned} \tag{15}$$

where $\boldsymbol{x}$ denotes design variables and $c(\boldsymbol{x})$, $p_f(\boldsymbol{x})$, p_f^t, and $\boldsymbol{X}$ respectively denote a cost function, a (conventional or buffered) failure probability, a target failure probability, and a feasible set of $\boldsymbol{x}$. Since the reliability constraint in Eq. (15) is often intractable, one can approximate the constraint by generating MC samples of $\boldsymbol{V}$. Then, with the conventional failure probability, Eq. (15) becomes

$$\begin{aligned} &\min_{\boldsymbol{x}} c(\boldsymbol{x}) \\ &\text{s.t. } \frac{1}{N}\sum_{i=1}^{N} \mathbb{I}\left[g(\boldsymbol{x}, \boldsymbol{v}^i) \ge 0\right] \le p_f^t \\ &\quad \boldsymbol{x} \in \boldsymbol{X}, \end{aligned} \tag{16}$$

where $\boldsymbol{v}^1, \ldots, \boldsymbol{v}^N$ are the MC samples of $\boldsymbol{V}$. On the other hand, when the buffered failure probability is used, Eq. (15) can be reformulated as

$$\begin{aligned} &\min_{\boldsymbol{x}, z_0, \boldsymbol{z}} c(\boldsymbol{x}) \\ &\text{s.t. } z_0 + \frac{1}{\bar{p}_f^t}\sum_{i=1}^{N} \frac{z_i}{N} \le 0 \\ &g(\boldsymbol{x}, \boldsymbol{v}^i) - z_0 \le z_i, \quad i = 1, \cdots, N \\ &\boldsymbol{x} \in \boldsymbol{X}, z_0 \in \mathbb{R}, z_i \in \mathbb{R}^+, \ i = 1, \cdots, N, \end{aligned} \tag{17}$$

where two types of auxiliary design variables, z_0 and $\boldsymbol{z} = (z_1, \cdots, z_N)$ are introduced (Rockafellar and Royset, 2010). In Eq. (17), z_0 corresponds to an estimation of quantile $q_{\bar{\alpha}_0}$ in Eq. (6), and z_i denotes the distance between a sample $g(\boldsymbol{x}, \boldsymbol{v}^i)$ and $q_{\bar{\alpha}_0}$.

Comparison between Eqs. (16) and (17) underlines computational advantages of the buffered failure probability over the conventional one, as analyzed by previous works (Basova et al., 2011; Byun et al., 2022; Royset, 2022). Those advantages arise from the fact that Eq. (17) does not involve the indicator function $\mathbb{I}[\cdot]$ as Eq. (16), whose 0-1 discontinuity hinders evaluating gradients of reliability constraints. This issue is critical for optimization problems since many algorithms require gradient information. While Eq. (17) introduces additional decision variables z_0 and $\boldsymbol{z}$, they do not add much computational cost as the formula is linear in these variables. Another advantage is that Eq. (17) handles $c(\boldsymbol{x})$ and $g(\boldsymbol{x}, \boldsymbol{v}^i)$ as they are, whereby computational complexity is determined by the functions themselves. In other words, if $c(\boldsymbol{x})$ and $g(\boldsymbol{x}, \boldsymbol{v}^i)$ have good properties, these properties are preserved. For example, if the functions are

continuously differentiable with respect to $\boldsymbol{x}$, Eq. (17) is solvable by standard nonlinear optimization algorithms. If the functions are linear (convex) in $\boldsymbol{x}$, the formula becomes a linear (convex) optimization problem.

4.2. Numerical Comparison of RBO Solutions

This section investigates whether the two failure probabilities lead to the same RBO solutions when a target failure probability is properly scaled. If the contour maps of the two metrics on a solution domain have similar shapes, one can conclude that the two failure probabilities lead to similar optimization solutions. To this end, we consider a limit-state function

$$g(\boldsymbol{x}, \boldsymbol{V}) = S - \left(\frac{R}{\tau_R} + \mu_R\right), \tag{18}$$

where the random variables in $\boldsymbol{V} = (R, S)$ represent the capacity and demand of an engineering system, respectively. Since demand S is often uncontrollable, we set design variables as $\boldsymbol{x} = (\mu_R, \tau_R)$ representing the mean and the precision (i.e., the inverse of standard deviation) of R. The solution space is set to $\mu_R \in (2,5)$ and $\tau_R \in (0,4)$.

For comparison, we investigate various distributions of R and S, including the normal and lognormal distributions as representatives of light and heavy tail distributions, respectively. We also consider a multimodal shape by using a Gaussian mixture distribution. The parameters of the distributions are summarized in Table 1.

Table 1: Distribution parameters for R and S

Shape	Symbol	Distribution
Light tail	*L*	$\mathcal{N}(\mu, \sigma^2)$, $\mu = 0, \sigma = 1$
Heavy tail	*H*	$\mathcal{LN}(\lambda, \zeta^2)$, $\lambda = 0, \zeta = 1$
Multimodal	*M*	$\sum_{i=1}^{2} \phi_i \mathcal{N}(\mu_i, {\sigma_i}^2)$, $\phi_1 = 0.95, \phi_2 = 0.05$, $\mu_1 = 0, \mu_2 = 30$, $\sigma_1 = 1, \sigma_2 = 5$

The two failure probabilities are estimated by generating 10^6 MC samples, as shown in Figures 4 and 5. In Figure 4, the contours are drawn for different combinations of the light and heavy tail distributions, while Figure 5 illustrates contours with multimodal distributions combined with other distributions. In the figure, the failure probabilities are expressed in a decimal logarithm.

Figures 4 and 5 show that both probabilities generally decrease as μ_R and τ_R increase. In Figure 4, all figures show consistent contour shapes, which suggests that tail heaviness does not lead to different RBO solutions between the two failure probabilities. On the other hand, in Figure 5, the contours show notable differences, particularly in the red boxes in the second and third columns. This suggests that, in contrast to tail heaviness, multi-modality can lead to different decision preferences of the two failure probabilities.

5. CONCLUSIONS

This paper presents comparative investigations of the conventional and buffered failure probabilities. In general, we observed that the two reliability metrics are fundamentally equivalent from the risk management perspective as both represent the likelihood of the worst scenarios, i.e., failure events. Nonetheless, they define failure events differently, resulting in notable differences. First, the two failure probabilities are based on different perspectives on failure probabilities. The conventional failure probability does not consider the magnitude of a failure event, while the buffered failure probability does. This observation suggests that the two reliability metrics are more suitable for different problems. Nonetheless, as the two metrics show strongly positive correlations, their interchangeable use seems possible in most cases. Second, while different mathematical expressions are used to calculate the two metrics, the buffered failure probability tends to demand more complicated formulas. We also observed that when Monte Carlo Simulation (MCS) is employed for calculations, the buffered failure probability is highly likely to underestimate the failure

probability when the sample size is small, which is not the case for the conventional failure probability. Third, the computation becomes more manageable in reliability-based optimization if the buffered failure probability is adopted, as its calculation does not cause 0-1 discontinuity.

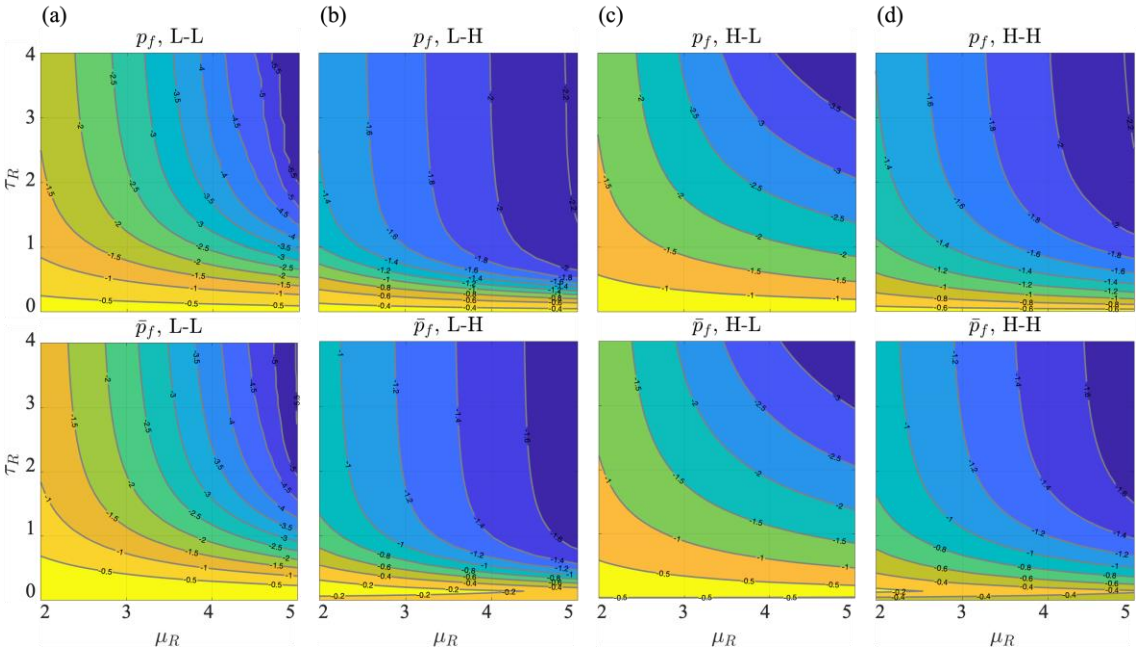

Figure 4: Contour maps of p_f and $\bar{p}_f$ with different combinations of light and heavy-tailed distributions. Distributions of R and S are represented by symbols to the left and right of the hyphen.

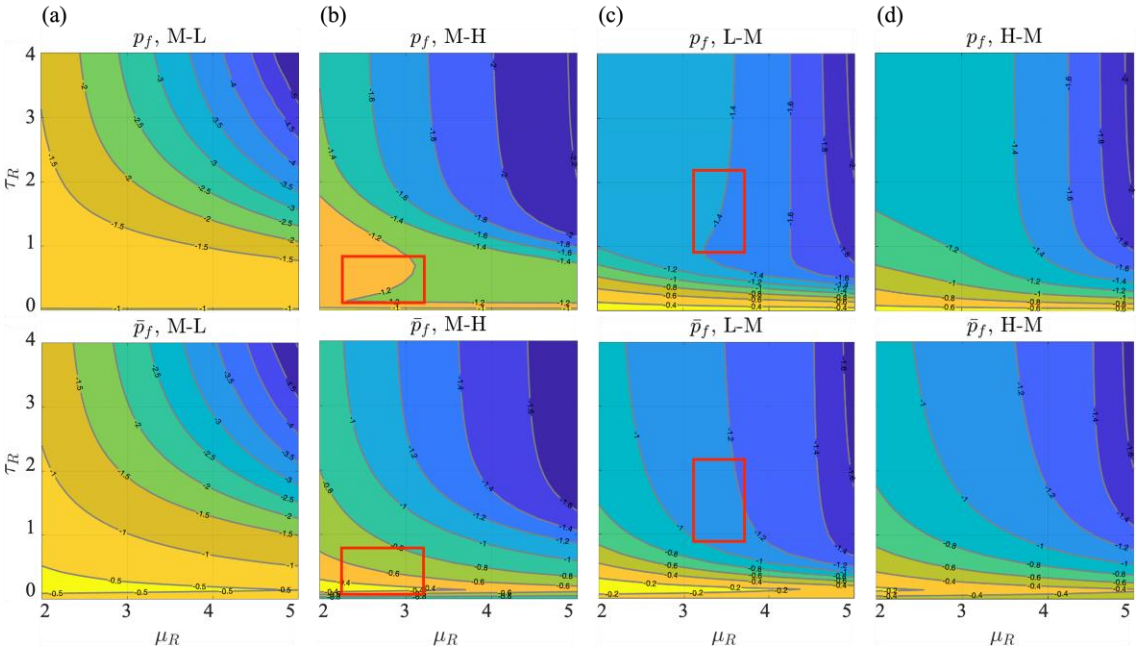

Figure 5: Contour maps of p_f and $\bar{p}_f$ with different combinations of multimodal distributions and other distributions. The red boxes in (b) and (c) indicate where the contour maps show a distinctive discrepancy.

Meanwhile, we observed that the two failure probabilities lead to similar contour maps of failure probability over a solution space. This observation implies that they generally lead to similar optimization solutions when a target failure probability is properly scaled (since the buffered failure probability is always equal to or greater than the conventional one). However, contour maps may show discrepancies when a random variable follows a multimodal distribution. On the other hand, such a discrepancy is not contingent on the tail-heaviness of a distribution.

The general similarity between the two reliability metrics increases the potential for their complementary uses. This is especially appealing because the mathematical properties of the two metrics compensate for each other: the conventional failure probability simplifies probability calculations, and the buffered failure probability facilitates reliability-based optimization. Such parallel use can be enabled by drawing consensus on permissible levels of the buffered failure probability for a discipline of interest, which widely exists for the conventional probability. Another prospect is to develop advanced inference techniques for buffered failure probability, such as sampling and surrogate modeling.

6. ACKNOWLEDGEMENT

This work is supported by the Korea Agency for Infrastructure Technology Advancement (KAIA) grant funded by the Ministry of Land, Infrastructure and Transport (Grant RS-2021-KA163162) and is financially supported by Korea Ministry of Land, Infrastructure and Transport(MOLIT) as Innovative Talent Education Program for Smart City. The second author is supported by the Alexander von Humboldt Foundation.

7. REFERENCES

Basova, H.G., Rockafellar, R.T., & Royset, J.O. (2011). A computational study of the buffered failure probability in reliability-based design optimization. *In Proc. 11th Conf. Appl. Statist. Probab. Civil Engrg., Zurich, Switzerland*.

Betz, W. (2017). *Bayesian inference of engineering models* (Doctoral dissertation, Technische Universität München).

Byun, J.E., de Oliveira, W., & Royset, J.O. (2022). S-BORM: Reliability-based optimization of general systems using buffered optimization and reliability method. *arXiv preprint arXiv:2209.02573*.

Byun, J.E., & Royset, J.O. (2022). Data-driven optimization of reliability using buffered failure probability. *Structural Safety*, *98*, 102232.

Der Kiureghian, A. (2022). *Structural and System Reliability*, Cambridge University Press, New York, NY.

Mafusalov, A., & Uryasev, S. (2018). Buffered probability of exceedance: mathematical properties and optimization. *SIAM Journal on Optimization*, *28*(2), 1077-1103.

Mafusalov, A., Shapiro, A., & Uryasev, S. (2018). Estimation and asymptotics for buffered probability of exceedance. *European Journal of Operational Research*, 270(3), 826-836.

Rockafellar, R.T., & Royset, J.O. (2010). On buffered failure probability in design and optimization of structures. *Reliability engineering & system safety*, *95*(5), 499-510.

Rockafellar, R.T., & Royset, J.O. (2015). Engineering decisions under risk averseness. *ASCE-ASME Journal of Risk and Uncertainty in Engineering Systems, Part A: Civil Engineering*, *1*(2), 04015003.

Rockafellar, R.T., & Uryasev, S. (2000). Optimization of conditional value-at-risk. *Journal of risk*, *2*, 21-42.

Rockafellar, R.T., & Uryasev, S. (2002). Conditional value-at-risk for general loss distributions. *Journal of banking & finance*, *26*(7), 1443-1471.

Royset, J.O. (2022). Risk-Adaptive Approaches to Learning and Decision Making: A Survey. *arXiv preprint arXiv:2212.00856*.

Royset, J.O., & Byun, J.E. (2021). Gradients and subgradients of buffered failure probability. *Operations Research Letters*, *49*(6), 868-873.